

Broadband characterization of stress induced anisotropy in nanocomposite $\text{Co}_{74.6}\text{Fe}_{2.7}\text{Mn}_{2.7}\text{Nb}_4\text{Si}_2\text{B}_{14}$

Abhishek Srivastava¹, Kayla Cole¹, Alicia Wadsworth², Thomas Burton², Claudia Mewes¹,
Tim Mewes¹, Gregory B. Thompson², Ronald D. Noebe³, and Alex M. Leary³

¹Department of Physics and astronomy, The University of Alabama, Tuscaloosa, AL 34501,
USA

²Department of Metallurgical and Materials Engineering, The University of Alabama,
Tuscaloosa, AL 34501, USA

³Materials and Structures Division, NASA Glenn Research Center, Cleveland, OH 44135,
USA

Abstract

We report on the broadband characterization of $\text{Co}_{74.6}\text{Fe}_{2.7}\text{Mn}_{2.7}\text{Nb}_4\text{Si}_2\text{B}_{14}$ (at%) melt-spun, soft magnetic alloy ribbons after various secondary processing treatments. Ribbons were investigated in the as-cast (melt-spun) condition, after annealing under stress at 50 – 200 MPa, and after transverse magnetic field (TMF) annealing. The magnetization dynamics of these materials have been studied from 10 - 60 GHz using ferromagnetic resonance (FMR). The in-plane uniaxial anisotropy was determined from the FMR data and permeability extracted for each condition. The permeability determined from broadband FMR was in good agreement with independently determined values using vibrating sample magnetometry and impedance spectrometry of toroidal cores. The effective damping parameter (α_{eff}) of all the samples was close to 0.015 except for the TMF sample, which showed higher damping, possibly due to two magnon scattering.

1 Introduction

Nanocomposite soft magnetic materials consist of nanocrystalline grains dispersed in an amorphous matrix [1]. The principle method for forming this type of material is to start with an amorphous precursor, usually melt spun ribbon, followed by thermal annealing, which partly devitrifies the material. One variation on this technique is to apply a stress to the ribbon while annealing the material, which provides an added benefit of being able to induce a controlled magnetic anisotropy. By changing the annealing conditions and the stress during annealing the magnitude of the induced anisotropy [2] as well as easy axis of the anisotropy can be tuned [3]. Co-rich nanocomposites exhibit an increased relative strain at fracture when compared to Fe-based nanocomposites [4], and have recently been shown to be excellent candidates for in-line stress-annealing techniques [1].

The permeability of nanocomposites is one of the key material parameters that determines their usefulness for inductive components in high power electronics, transformers and electrical motors. In this article, we report on permeability measurements of $\text{Co}_{74.6}\text{Fe}_{2.7}\text{Mn}_{2.7}\text{Nb}_4\text{Si}_2\text{B}_{14}$ (at%) after various annealing conditions using three different methods, vibrating sample magnetometry (VSM), impedance measurements of toroidal cores, and ferromagnetic resonance (FMR), and found the results to be in close agreement. This establishes FMR as an alternative method to determine the permeability of nanocomposite ribbons, while at the same time probing the high frequency dynamics of the materials. The method can be adapted for nondestructive permeability measurements by correcting for geometrical effects and might enable in-situ permeability measurement providing an advantage over conventional methods, which are destructive in nature.

High frequency damping characteristics are another important parameter for these types of soft magnetic materials when considered for applications like electromagnetic shielding [5] and high frequency power conversion [6]. Due to its high magnetic moment and soft magnetic properties, Co-base alloys, such as the $\text{Co}_{74.6}\text{Fe}_{2.7}\text{Mn}_{2.7}\text{Nb}_4\text{Si}_2\text{B}_{14}$ studied here, can also be used as a soft magnetic underlayer for magnetic flux concentration in perpendicular recording systems, for which the high frequency response is particularly important [7, 8]. We have extracted the effective damping parameter (α_{eff}) and inhomogeneous linewidth broadening (ΔH_0) from broadband FMR measurements, which show that both parameters are unaffected by stress annealing and are not significantly different from the as-cast samples. However, for samples annealed in a transverse magnetic field we find a significantly enhanced effective damping and inhomogeneous linewidth broadening.

2 Experimental techniques

Amorphous Co_{74.6}Fe_{2.7}Mn_{2.7}Nb₄Si₂B₁₄ (at%) ribbon, approximately 25 mm wide and 22 microns thick, was produced using a pilot-scale, planar-flow melt spin system. Melting and casting were performed in air under an inert gas-shrouded environment. In addition to studying the as-cast amorphous ribbon, two secondary annealing treatments were applied in air to the as-cast ribbon to produce different nanocomposite structures:

1. Transverse magnetic field annealing (TMF) at 540 °C for 1 hr with a 2 T magnetic field applied perpendicular to the ribbon long axis in the ribbon plane.
2. Stress annealing (SA) where sections of the ribbon were annealed while moving through a furnace at 560 °C under various tensions (50 to 200 MPa). Segments of ribbon underwent heating for approximately 5 seconds during this in-line anneal.

The saturation magnetization, M_s , of the as-cast and annealed materials were measured using a Lake Shore 7400 Vibrating Sample Magnetometer (VSM). Density of the as-cast and annealed material is $\rho = 8.35 \pm 0.05$ g/cc and accuracy of specific magnetization was within ± 1 Am²/kg for the ~20 mg samples, resulting in a 1.7% accuracy for the measured induction values (B) from the VSM data. FMR measurements were performed on a custom system that utilizes a coplanar waveguide (CPW), capable of exciting the sample with a microwave field between 1 to 65 GHz [9]. FMR measurements used a fixed microwave frequency and swept the external applied field to obtain resonance in the sample. Power transmitted through the sample located on the CPW is detected using a Schottky diode with a lock-in technique by adding a small modulation field to the applied field [10]. For the measurements on the nanocomposite ribbons, the modulation frequency was $f_{mod} = 800$ Hz and the modulation field, $\mu_0 H_{mod}$, was varied linearly with microwave frequency from 2 mT at 10 GHz to 4 mT at 56 GHz.

Three different techniques were used to measure magnetic anisotropy and permeability; impedance measurements on wound cores, in plane FMR using 6 mm discs, and in plane VSM using 3 mm discs. Impedance spectra of TMF and SA toroidal cores with cross section A_c and path length ℓ , were wound with two $N = 50$ turn bifilar windings and were measured using a Keysight E4990A Impedance Analyzer. Material permeability was determined using the measured equivalent series inductance at 10 kHz from the primary winding with the secondary winding open (L_o) and shorted (L_s). The measured inductance $L_m = L_o - L_s$ corrects for the leakage effects and the relative permeability μ_r is obtained from $L_m = N^2 A_c \mu_r \mu_0 / \ell$ with μ_0 equal to the permeability of free space. In-plane FMR and VSM measurements used disc samples punched from ribbons and mounted to the flat end of a glass rod that is free to rotate about its axis by a servo motor. Figure 1

describes the coordinate system of the large, quasi-DC applied field that was swept over the resonance field at a fixed frequency in the FMR and swept between positive and negative values that saturated the disc sample in the VSM to measure hysteresis. Both in plane techniques varied the field angle θ to achieve a full 360° rotation with 5° increments, where $\theta = 0^\circ$ orients the quasi-DC field parallel to the long axis of the ribbon, which was also the direction of applied stress during stress annealing. Anisotropy values from the FMR and VSM techniques were derived from measured values as described below.

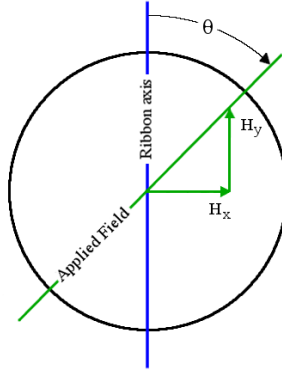


Figure 1: Coordinate system describing the applied DC field for in-plane disc measurements.

3 Results

Figure 2a shows a typical FMR spectrum at $\theta = 0^\circ$ and a fit using the first derivative of a Lorentzian with both absorptive and dispersive contributions [11, 12]. From this fit, the resonance field, H_{res} , and the linewidth, ΔH , are determined. In this example, the resonance field $\mu_0 H_{res} = 1.1$ T and linewidth $\mu_0 \Delta H_{PP} = 44.3$ mT for a 3 mT modulation field at 800 Hz. By measuring the H_{res} over a broad frequency range one obtains the data shown in figure 2b. This data is well described by the Kittel equation (Eq. 1) for a material with a uniaxial in-plane anisotropy, K_u , measured along the hard-axis [13, 14].

$$f = \mu_0 \cdot \gamma' \sqrt{[H_{res} - H_u] [H_{res} + M_{eff}]} \quad (1)$$

Where M_{eff} is the effective magnetization, the reduced gyromagnetic ratio $\gamma' = \frac{\gamma}{2\pi}$, and the in-plane uniaxial anisotropy field $H_u = \frac{2K_u}{\mu_0 M_s}$ where K_u is the uniaxial anisotropy constant and M_s is the saturation magnetization . The effective magnetization accounts for both the shape anisotropy of the disc and the perpendicular anisotropy and is given by

$$M_{eff} = M_s - \frac{2K_\perp}{\mu_0 M_s} \quad (2)$$

where M_s is the saturation magnetization and K_\perp is the out-of-plane perpendicular anisotropy of the ribbon. For samples with $K_\perp = 0$ the effective magnetization is equal to the saturation magnetization of the sample. The values of M_{eff} and γ' , obtained by fitting the experimental data using Eq. 1, are summarized in Table 1 and shown in figure 3. The effective magnetization (figure 3a) for the as-cast sample is slightly higher than the stress annealed samples and no significant dependence on the stress during annealing is observed. Also, the gyromagnetic ratio (figure 3b) remained constant within the error margin for all samples.

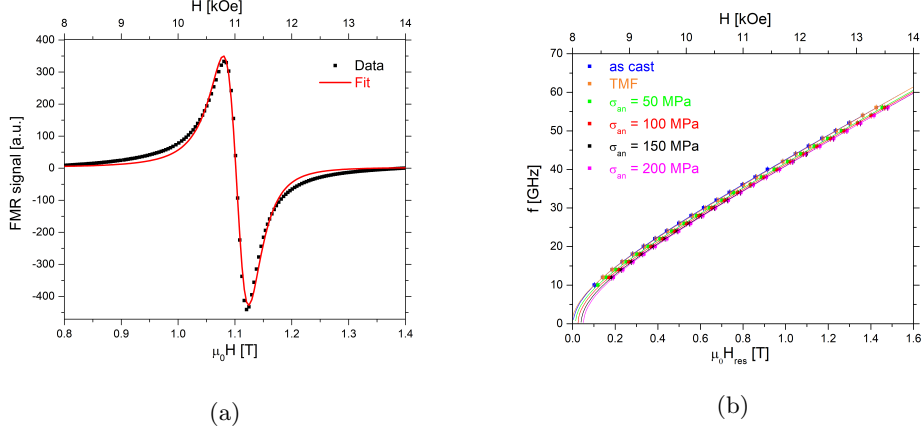


Figure 2: a) Field swept FMR spectrum measured at 46 GHz for a sample stress annealed at 100 MPa. b) Frequency dependence of FMR resonance field of all the samples. The continuous lines represent the fit to the experimental data using Eq. 1.

While the fit of broadband FMR data also results in a parameter for the anisotropy field, H_u , in the sample, this value should only be considered a rough estimate of the anisotropy field. For completeness these values are listed in Table 1 with the label 'Kittel'. Because the measurements were only carried out with the field applied along the spin-casting direction, no conclusion regarding the symmetry of the anisotropy can be derived from those measurements alone. However, as can be seen in figure 2b the ferromagnetic resonance frequency drops to zero at finite positive fields indicating that this is a hard axis of the sample. Furthermore, we note that the magnitude of H_u , determined in this fashion, will sensitively depend on the relative alignment of the field with respect to the anisotropy axis of the sample. This systematic error is not included in the error margins in Table 1, which are based solely on the statistical error of the anisotropy field. The correlation of the different fit parameters in Eq. 1 further adds to the uncertainty of this value. Thus in order to obtain precise values for H_u , we have performed in-plane angle dependent FMR measurements for all samples, which clearly show the uniaxial nature of the anisotropy.

The nature of the magnetic anisotropy becomes evident by varying θ during FMR measurements. For the as-cast and TMF samples, the FMR technique shows no significant in-plane anisotropy, as is evident in figure 4 (a) and (b), respectively. Stress annealed samples do show clear minima in the angular variation of the

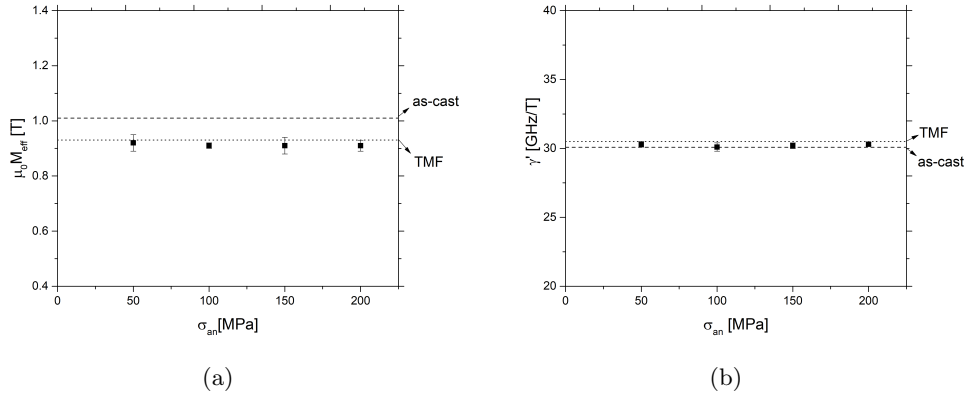


Figure 3: (a) Effective magnetization, M_{eff} , and (b) the reduced gyromagnetic ratio, γ' , extracted from broadband FMR measurements for all the samples. The data points represent the different stress annealed conditions, the dashed horizontal line represents the corresponding parameters of the as-cast ribbon, and dotted line corresponds to the ribbon sample annealed in a transverse magnetic field (TMF).

@ 300 K	as-cast	stress annealed at 50 MPa	stress annealed at 100 MPa	stress annealed at 150 MPa	stress annealed at 200 MPa	annealed in TMF
$\mu_0 M_{eff}$ [T]	1.01 ± 0.01	0.92 ± 0.03	0.91 ± 0.05	0.91 ± 0.03	0.91 ± 0.02	0.93 ± 0.01
γ' [GHz/T]	30.08 ± 0.07	30.3 ± 0.2	30.26 ± 0.03	30.21 ± 0.02	30.36 ± 0.01	30.50 ± 0.05
$\mu_0 H_u$ (Kittel)[mT]	4 ± 1	14 ± 3	25.6 ± 0.6	39.9 ± 0.4	51 ± 3	-3 ± 1
$\mu_0 H_u$ (in-plane rotation)[mT]	0 ± 2	13.6 ± 0.1	26.3 ± 0.2	36.2 ± 0.2	41.1 ± 0.4	0 ± 4

Table 1: Parameters extracted from Kittel plot

resonance field, as shown in figures 4 (c)-(f), that indicate an easy direction near $\theta = 90^\circ$. Assuming that the magnetization is aligned with the externally applied field for all angles, i.e. $\theta_M = \theta$ and for $M_s > H_{res} \gg H_u$ an approximate analytic expression for the in-plane angular dependence of the resonance field is given by [14, 15, 16]:

$$H_{res} = H_0 - H'_u \cos(2(\theta_M - \theta_0)) \quad (3)$$

In this equation the angle of the magnetization, θ_M , is defined relative to the easy axis located at θ_0 . As noted above, the easy axis for the stress annealed samples is perpendicular to the direction of applied tensile stress, i.e., $\theta_0 = 90^\circ$. A fit of the experimental data using Eq. 3 is shown in figures 4 (c)-(f). While the parameter H'_u in Eq. (3) is often identified as the uniaxial anisotropy of the material, the assumptions underlying the derivation of this equation imply that $H'_u \neq H_u$, where H_u is the anisotropy field introduced

in Eq.(1)[14]. However, the two quantities are related by the following expressions:

$$\begin{aligned}
H_u &= \frac{1}{2} \left(-b + \sqrt{b^2 - 4c} \right) \quad \text{with} \\
b &= \frac{1}{8} \left(6\tilde{H}_u + 2M_{eff} \right), \\
c &= \frac{1}{8} \left(\tilde{H}_u^2 - 4\frac{f^2}{\gamma'^2} - M_{eff}^2 \right) \quad \text{and} \\
\tilde{H}_u &= \sqrt{M_{eff}^2 + 4\frac{f^2}{\gamma'^2} - 4H'_u}
\end{aligned} \tag{4}$$

Therefore by fitting the in-plane angular variation of resonance field, H_{res} , as a function of the direction of external magnetic field, using equations (3) and (4) we obtain the uniaxial anisotropy field in the material, H_u . These values are indicated in figure 4 and listed in Table 1 with the identifier 'in-plane rotation', the values $\mu_0 H_u$ range from 13.6 mT for the sample stress annealed at 50 MPa to 41.1 mT for the sample stress annealed at 200 MPa. The data in Table 1 also show that the statistical error margins of the uniaxial anisotropy field obtained from in-plane angle dependent measurements for the stress annealed samples is significantly lower than those obtained from frequency dependent data.

Broadband ferromagnetic resonance measurements also provide valuable information about the relaxation in the samples [17]. The analysis of this information is based on the frequency dependence of the linewidth, shown in figure 5. Based on Suhl's formula [18], which is valid when $\theta = \theta_M$, the frequency dependence of the linewidth is [19, 20, 21]:

$$\Delta H = \Delta H_0 + \frac{2}{\sqrt{3}} \cdot \alpha_{eff} \cdot \frac{f}{\gamma'} \tag{5}$$

Here, f is the microwave frequency, α_{eff} is the effective Gilbert damping parameter, ΔH is the peak-to-peak linewidth, ΔH_0 is the linewidth extrapolated to zero frequency, and γ' is the reduced gyromagnetic ratio. The parameters extracted from linewidth vs. frequency data are shown in figure 6. The damping coefficient, α_{eff} , for the as-cast and strain annealed samples are of the same order of magnitude (see figure 6b and Table 2) indicating that relaxation is not affected by stress annealing. Moreover, similar values of ΔH_0 (see figure 6a and Table 2) suggest that the magnetic inhomogeneity also does not depend on stress annealing of the material. However, both values are significantly different in the case of the transverse magnetic field annealed sample (Table 2). A nonlinear frequency dependence of the linewidth as observed for the TMF sample (see figure 5) is indicative of a strong two-magnon scattering [14, 22].

The saturation induction, $B_s = \mu_0 M_s$, measured using VSM, of the as-cast ribbon, the TMF, and 100 MPa SA samples were 1.01 T, 0.94 T, 0.99 T, respectively. Saturation induction is known to decrease

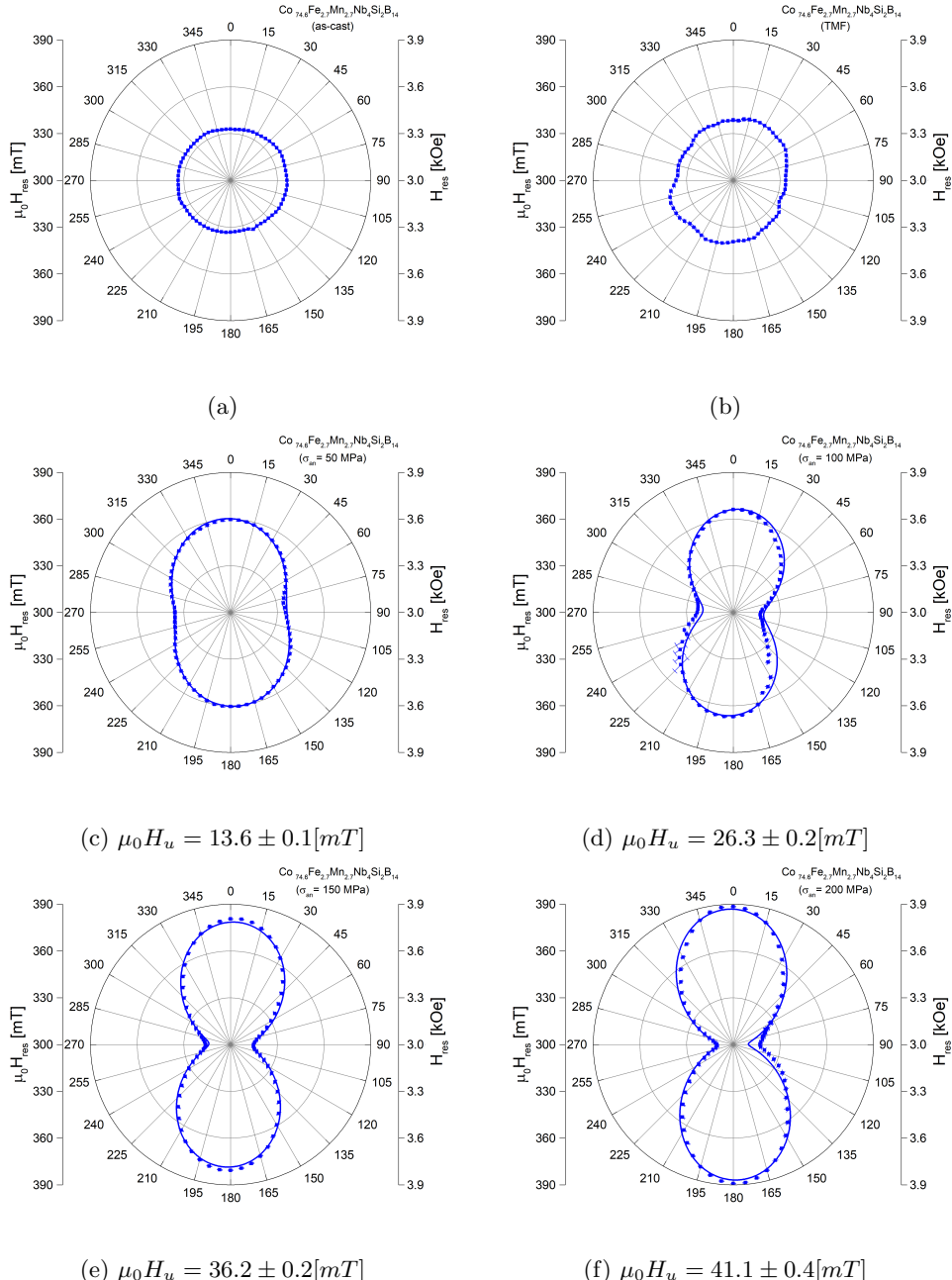


Figure 4: In-plane angular variation of resonance field at 20 GHz of a) as-cast, b) annealed in transverse magnetic field (TMF), c) stress annealed at 50 MPa, d) 100 MPa, e) 150 MPa and f) 200 MPa. Zero degree corresponds to the spin-casting direction and also the stress axis in SA samples. The experimental data is shown as blue squares, and the fit is shown as a continuous line.

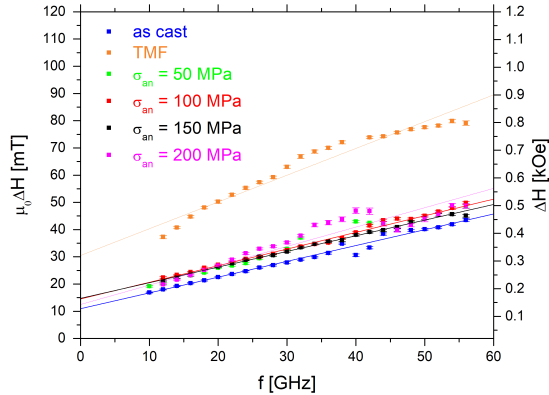


Figure 5: Frequency dependence of the FMR linewidth of all $\text{Co}_{74.6}\text{Fe}_{2.7}\text{Mn}_{2.7}\text{Nb}_4\text{Si}_2\text{B}_{14}$ samples. The continuous line is fit to the data using Eq. 5

@ 300 K	as-cast	stress annealed at 50 MPa	stress annealed at 100 MPa	stress annealed at 150 MPa	stress annealed at 200 MPa	annealed in TMF
$\mu_0 \Delta H_0 [\text{mT}]$	10.9 ± 0.4	13.2 ± 0.7	12.9 ± 0.6	19.2 ± 0.7	17.8 ± 0.6	30 ± 2
α	$0.0152 \pm 4\text{E-}4$	$0.0164 \pm 4\text{E-}4$	$0.0159 \pm 3\text{E-}4$	$0.0151 \pm 2\text{E-}4$	$0.019 \pm 1\text{E-}3$	$0.026 \pm 1\text{E-}3$

Table 2: Parameters extracted from linewidth vs frequency data

during annealing, as previously reported for this class of Co-rich materials [23], and longer annealing time above the primary crystallization temperature $\simeq 420$ °C, produce lower induction materials compared to shorter annealing times. Thus, the 1 hour treatment at 540 °C for the TMF sample significantly reduces the saturation induction compared to the as-cast material, while there is very little change after strain annealing, since the sample was at temperature for only about 5 seconds. The saturation values derived from FMR data (Table 1) agree well with B_s values measured using the VSM. It is worth mentioning in this context that FMR measurements do not require knowledge of the volume or mass of the sample but instead solely rely on precise measurements of the resonance field. Magnetic anisotropy can also be determined from torque measurements in a VSM equipped with at least two coils to detect orthogonal magnetization components [24]. The torque τ is produced by the magnetization perpendicular to the effective field that accounts for shape anisotropy as $\tau = \mu_0 M_\perp H_{eff}$. For magnetization oriented at θ_M from a uniaxial easy axis in the same plane, the energy is [25] $E_a = K_0 + K_{u,1}\sin^2(\theta_M) + K_{u,2}\sin^4(\theta_M) + \dots$ and the anisotropy constants can be derived by fitting the torque curve to a Fourier series. Anisotropy constants can also be calculated from a single magnetization curve if H_{eff} accounts for shape anisotropy [26]. While shape anisotropy is significant in the disc samples described here favoring an in-plane orientation of the magnetization over an out-of-plane orientation closure domains near the surface can stabilize bulk domains with significant out of plane orientations. Furthermore the shape anisotropy is isotropic in the plane of the disk. The proposed VSM

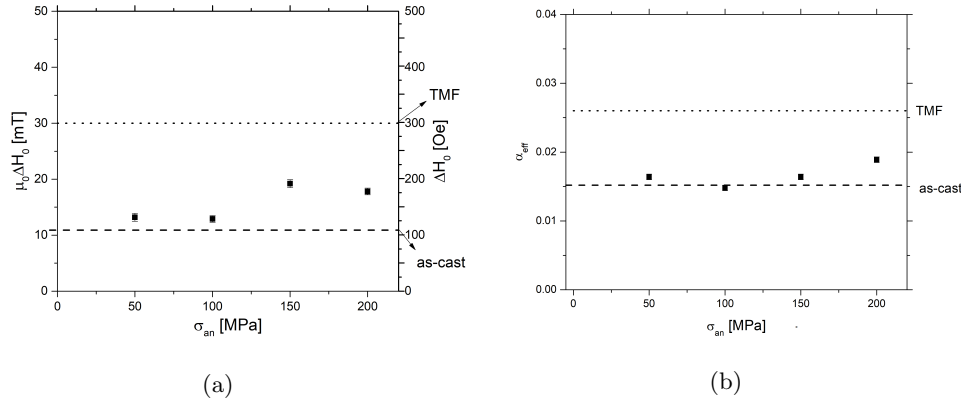


Figure 6: (a) Linewidth extrapolated to zero field and (b) effective damping constant extracted from the frequency dependence of linewidth, obtained from broadband FMR measurements for the as-cast Co_{74.6}Fe_{2.7}Mn_{2.7}Nb₄Si₂B₁₄ alloy and after different annealing treatments. The data points represent the different stress annealed conditions, the dashed horizontal line represents the corresponding parameters of the as-cast ribbon, and dotted line corresponds to the ribbon sample annealed in a transverse magnetic field (TMF).

technique does not require direct measurement of the demagnetizing fields and follows from the magnetic energy, given as:

$$E = E_{ex} + E_a + E_{sh} - \mathbf{M} \cdot \mathbf{H}. \quad (6)$$

where E_{ex} is exchange energy, E_a is anisotropy energy, E_{sh} is energy due to shape anisotropy and last term is the Zeeman energy.

In randomly oriented nanocomposites where the magnetocrystalline anisotropy is effectively averaged, the exchange energy E_{ex} is isotropic and the shape anisotropy E_{sh} for the disc geometry of our sample is also isotropic in the ribbon plane. Consequently, the induced anisotropy energy K_u can be measured using the VSM by comparing the susceptibility ($\chi = \frac{dM}{dH}$) of discs magnetized across different in-plane directions as in Eq. 7, which assumes constant χ to saturation.

$$\frac{1}{\chi_{hard}} - \frac{1}{\chi_{easy}} = \frac{1}{M_s} (H_{k,hard} - H_{k,easy}) \quad (7)$$

As all the energy terms are isotropic in the plane of the disc for $H \rightarrow 0$ the energy difference between easy and hard axis $E_{hard} - E_{easy} = \Delta K_u$. With $\Delta K_u = \frac{1}{2} \mu_0 M_s (H_{k,hard} - H_{k,easy})$, one has

$$\Delta K_u = \frac{\mu_0 M_s^2}{2} \left(\frac{1}{\chi_{hard}} - \frac{1}{\chi_{easy}} \right). \quad (8)$$

With the permeability of free space $\mu_0 = 4\pi \times 10^{-7} \text{ m} \cdot \text{kg} / \text{s}^2 \cdot \text{A}^2$. The saturation magnetization $M_s = \rho \cdot \sigma_s$

(σ_s : mass magnetization) is determined by saddling the sample between the VSM poles and applying a saturating field. Small sample movement from the initial saddled position, as θ varies, can be detected by monitoring $\sigma_s(\theta)$ under sufficiently high fields. This misalignment creates an error in the measured magnetization that can be corrected by scaling the measured data by the saddled, saturated value. Figure 7a shows σ vs H measurements along the easy and hard directions of an SA 100 MPa sample. The applied field at each θ varies as $H = \sqrt{H_x^2 + H_y^2}$ as shown in Figure 1 and χ at each radial field position on the positive portion of the hysteresis loop can be plotted to show the K_u symmetry in the material. Figure 7 b and c show radial susceptibility plots of 100 MPa SA and TMF samples, respectively, where the ribbon axis runs parallel to the $\theta = 0$ direction. Darker colors correspond to lower permeability with the black regions illustrating the saturating fields with respect to θ . Both materials show uniaxial symmetry and the SA material requires a higher saturating field along the ribbon axis direction compared to the TMF material.

Equation 8 is only valid if the angle dependent energy is dominated by the induced anisotropy. This is checked by comparing the energy product $M(\theta)H(\theta)$ where M is the measured magnetization of the sample and H is the external applied field. If $M(\theta)H(\theta)$ is proportional to $\chi_{hard} + \Delta\chi \cdot \sin^2 \theta$ at a fixed H value, the conditions required for Equation 8 are satisfied. Consequently the susceptibilities for Eq. 8 can be determined by fitting $\chi_{hard} + \Delta\chi \cdot \sin^2 \theta$ function to the χ vs θ values at $H \rightarrow 0$, where $\Delta\chi = \chi_{easy} - \chi_{hard}$.

Figure 8 shows fits to data at 100 A/m that yield $\chi_{hard} = 82.0 \pm 0.6$ and $\chi_{easy} = 117.0 \pm 0.6$ for the TMF sample and $\chi_{hard} = 27.5 \pm 0.5$ and $\chi_{easy} = 106.0 \pm 0.5$ for the 100 MPa SA sample. The corresponding K_u values are 1294 ± 40 J/m³ for the TMF and 10475 ± 350 J/m³ for the 100 MPa SA samples. The susceptibility measured along the easy axis is slightly lower than the maximum effective susceptibility expected for the disc shaped samples $\chi_{easy,max} = \frac{1}{N_{||}} = 143$, where $N_{||} = N_{xx} = N_{yy} = 0.007$ is the in-plane component of the demagnetizing tensor. This is expected as defects in the samples will reduce the measured susceptibility. Taking $\mu_r = 1 + \frac{M_s}{H_u} \approx \frac{M_s}{H_u}$ yields $\mu_r = 274 \pm 15$ for the TMF sample and $\mu_r = 37.2 \pm 1.8$ for the 100 MPa SA sample, as derived using the VSM technique. The relative permeability value is an intrinsic material property.

relative permeability at 300K	stress annealed at 50 MPa	stress annealed at 100 MPa	stress annealed at 150 MPa	stress annealed at 200 MPa	stress annealed at 250 MPa	TMF
Toroid method	73 ± 4	43 ± 2	32 ± 2	26 ± 1	23 ± 1	262 ± 5
VSM method	-	37 ± 2	-	-	-	274 ± 15
FMR method	69 ± 2	36 ± 2	26 ± 1	23 ± 1	-	-

Table 3: Permeability obtained using the toroid method, vibrating sample magnetometry (VSM), and ferromagnetic resonance (FMR). In the case of the FMR results, the effective magnetization of the respective sample obtained using broadband FMR was used to calculate the value listed in the table.

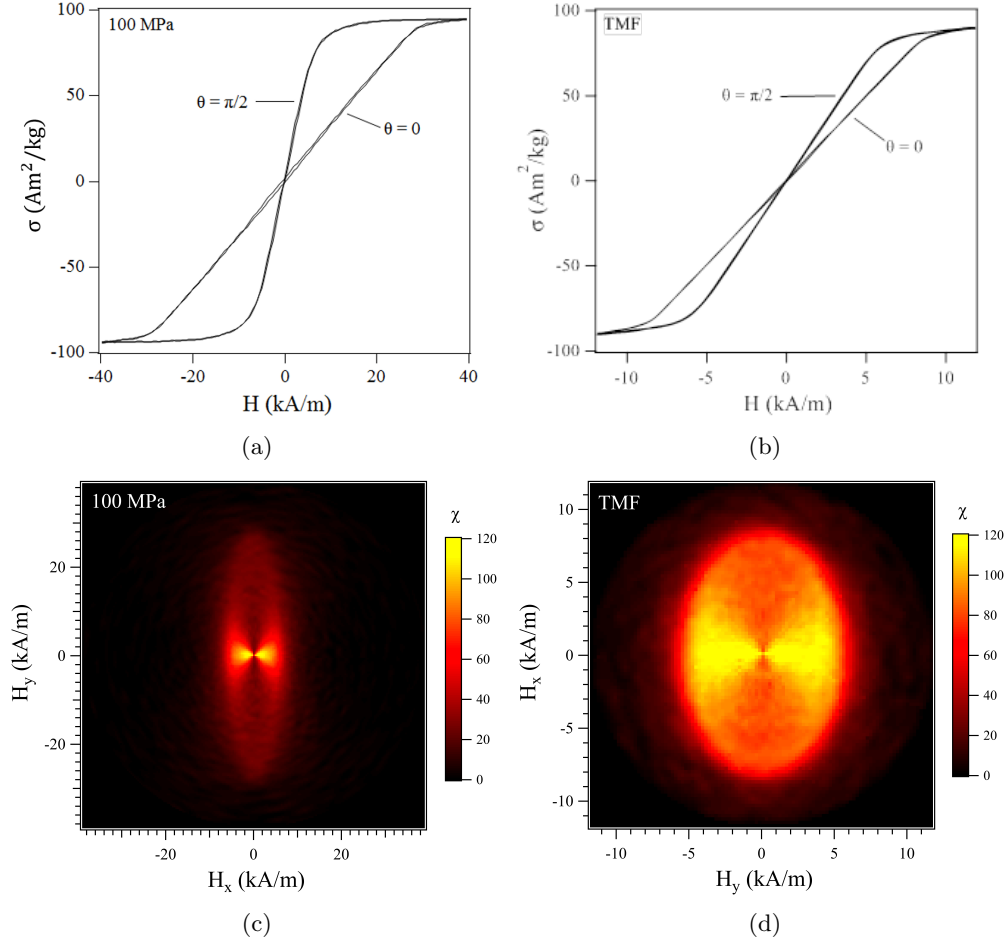


Figure 7: Hysteresis curves from a) 100 MPa SA sample and b) TMF sample measured with the field applied along the easy ($\theta = \frac{\pi}{2}$) and hard directions ($\theta = 0$). Radial susceptibility χ plots for c) SA and d) TMF samples, which show the symmetry of the induced anisotropy and saturating fields.

4 Discussion

The influence of the stress level during the annealing process on the uniaxial anisotropy field for $\text{Co}_{74.6}\text{Fe}_{2.7}\text{Mn}_{2.7}\text{Nb}_4\text{Si}_2\text{B}_{14}$ as determined using in-plane angle dependent FMR, is shown in figure 9. For comparison the values determined from broadband FMR measurements (black), are also shown. As discussed earlier, the values from broadband FMR can only serve as a rough estimate of the true anisotropy as they not only have larger statistical error margins, but also suffer from systematical errors like misalignment of the sample. Thus for the following discussion we focus on the uniaxial anisotropy field values, H_u , determined from in-plane rotation measurements.

For $\text{Co}_{74.6}\text{Fe}_{2.7}\text{Mn}_{2.7}\text{Nb}_4\text{Si}_2\text{B}_{14}$ the uniaxial magnetic anisotropy increases with increasing stress during the annealing process, at least over the levels of stress investigated. Thus the magnetic anisotropy induced by stress annealing in these nanocomposite ribbons can be tuned over a wide range. In typical applications

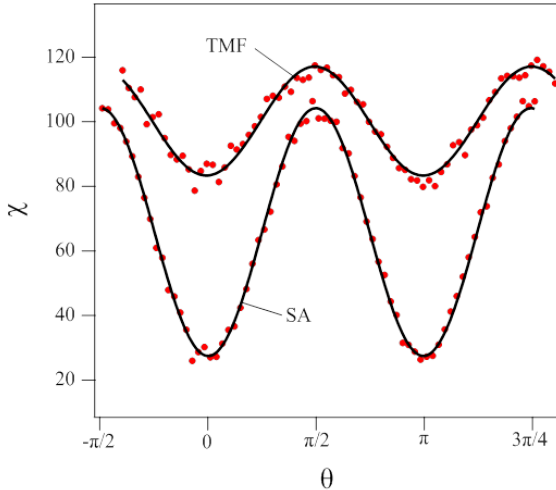


Figure 8: Angle dependent susceptibility χ , measured using VSM at $H = 100\text{A/m}$ for $\text{Co}_{74.6}\text{Fe}_{2.7}\text{Mn}_{2.7}\text{Nb}_4\text{Si}_2\text{B}_{14}$ TMF and 100 MPa SA samples. Fits correspond to $\chi_{hard} + \Delta\chi \cdot \sin^2 \theta$.

the relative magnetic permeability, μ_r , of the material in small fields applied along the hard axis is of particular importance. In this configuration one expects the magnetization reversal to be determined by rotation of the magnetization from the easy axis of the material toward the field direction [27, 28], resulting in a nearly constant permeability up to saturation, which in this model occurs at $H_s = H_u$. With this, one can determine the permeability of the samples using FMR measurement as $\mu_r = 1 + \frac{M_{eff}}{H_u}$. The resulting permeabilities are shown in figure 10 and in Table 3 in comparison with the results from VSM and the toroid method. The permeability in the SA samples determined using the toroid method is systematically higher than those determined using the other methods. Possible reasons for this include the assumption of a constant permeability until saturation that is used for both the VSM and FMR analyses and any stress induced in the core during winding. This stress can lead to a permeability measured using the toroid method that is different from the intrinsic value of the ribbon material [29, 30]. Given these possible issues, the agreement between the different methods is actually very good.

5 Conclusion

In summary we have studied $\text{Co}_{74.6}\text{Fe}_{2.7}\text{Mn}_{2.7}\text{Nb}_4\text{Si}_2\text{B}_{14}$, a soft magnetic alloy in the as-cast (melt-spun) condition, after stress annealing at 50–200 MPa and after annealing in a transverse magnetic field. In addition to the established toroid and VSM methods we have shown that broadband FMR provides an alternative method to determine the permeability of soft magnetic materials. Similar to the VSM method the FMR method is based on a linear approach to saturation or constant susceptibility.

By combining frequency dependent FMR measurements with in-plane angle dependent measurements we

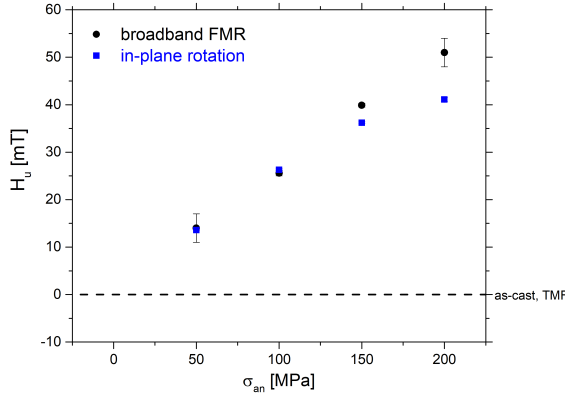


Figure 9: Dependence of the uniaxial anisotropy field, H_u , on the stress during annealing. Data obtained from broadband FMR measurements are shown as black symbols whereas the more precise data obtained from in-plane angle dependent measurements are shown in blue.

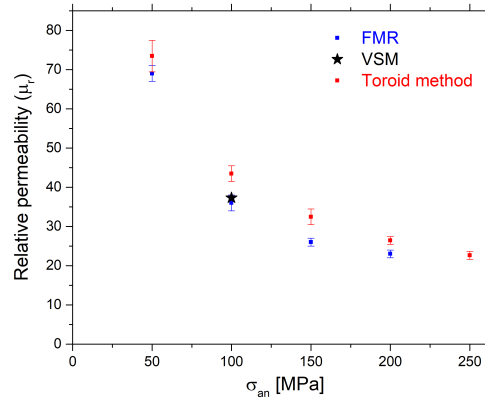


Figure 10: Comparison of the relative permeability as a function of the stress during annealing determined using the toroid method, VSM, and using the anisotropy field (H_u) obtained from FMR, assuming $M_s = M_{eff}$.

were able to achieve good agreement of the extracted susceptibility with the other methods.

In addition, broadband FMR also provides precise information regarding the effective magnetization, gyromagnetic ratio and damping of the material. The damping parameter plays a particularly important role for the potential use of these materials in high frequency applications.

Acknowledgement

The authors gratefully acknowledge funding for this research under the NASA Grant NASA CAN80NSSC18M0023. Additional support for this work came from the Advanced Air Transport Technology Project in the NASA

Advanced Air Vehicles Program. R.D.N and A.M.L also acknowledge useful discussions and experimental support from K. Beyerly, R. Bowman, V. Keylin, and G. Feichter.

References

- [1] K. Byerly, P. Ohodnicki, S. Moon, A. Leary, V. Keylin, M. McHenry, S. Simizu, R. Beddingfield, Y. Yu, G. Feichter, *et al.*, ‘‘Metal amorphous nanocomposite (MANC) alloy cores with spatially tuned permeability for advanced power magnetics applications,’’ *JOM*, vol. 70, pp. 879–891, 2018.
- [2] A. Leary, V. Keylin, P. Ohodnicki, and M. McHenry, ‘‘Stress induced anisotropy in cofemn soft magnetic nanocomposites,’’ *Journal of Applied Physics*, vol. 117, no. 17, p. 17A338, 2015.
- [3] O. Nielsen and H. Nielsen, ‘‘Magnetic anisotropy in $\text{Co}_{73}\text{Mo}_2\text{Si}_{15}\text{B}_{10}$ and $(\text{Co}_{0.89}\text{Fe}_{0.11})_{72}\text{Mo}_3\text{Si}_{15}\text{B}_{10}$ metallic glasses, induced by stress-annealing,’’ *Journal of Magnetism and Magnetic Materials*, vol. 22, no. 1, pp. 21–24, 1980.
- [4] T. Heil, K. Wahl, A. Lewis, J. Mattison, and M. Willard, ‘‘Nanocrystalline soft magnetic ribbons with high relative strain at fracture,’’ *Applied physics letters*, vol. 90, no. 21, p. 212508, 2007.
- [5] Y. Yang, B. Liu, D. Tang, B. Zhang, M. Lu, and H. Lu, ‘‘Influence of the magnetic field annealing on the extrinsic damping of fecob soft magnetic films,’’ *Journal of Applied Physics*, vol. 108, no. 7, p. 073902, 2010.
- [6] A. M. Leary, P. R. Ohodnicki, and M. E. McHenry, ‘‘Soft magnetic materials in high-frequency, high-power conversion applications,’’ *Jom*, vol. 64, no. 7, pp. 772–781, 2012.
- [7] H. Okumura, D. Twisselmann, R. D. McMichael, M. Huang, Y. Hsu, D. Laughlin, and M. McHenry, ‘‘Magnetic and structural characterization and ferromagnetic resonance study of thin film hitperm soft magnetic materials for data storage applications,’’ *Journal of applied physics*, vol. 93, no. 10, pp. 6528–6530, 2003.
- [8] C.-k. Lim, E.-s. Kim, and H.-s. Oh, ‘‘Perpendicular magnetic recording medium with controlled damping property of soft magnetic underlayer,’’ July 26 2007. US Patent App. 11/657,595.
- [9] B. Khodadadi, J. B. Mohammadi, J. M. Jones, A. Srivastava, C. Mewes, T. Mewes, and C. Kaiser, ‘‘Interlayer exchange coupling in asymmetric Co-Fe/Ru/Co-Fe trilayers investigated with broadband temperature-dependent ferromagnetic resonance,’’ *Physical Review Applied*, vol. 8, no. 1, p. 014024, 2017.
- [10] C. P. Poole, *Electron spin resonance: a comprehensive treatise on experimental techniques*. Courier Corporation, 1996.

- [11] C. J. Oates, F. Y. Ogrin, S. L. Lee, P. C. Riedi, G. M. Smith, and T. Thomson, “High field ferromagnetic resonance measurements of the anisotropy field of longitudinal recording thin-film media,” *Journal of Applied Physics*, vol. 91, no. 3, pp. 1417–1422, 2002.
- [12] N. Pachauri, B. Khodadadi, A. V. Singh, J. B. Mohammadi, R. L. Martens, P. R. LeClair, C. Mewes, T. Mewes, and A. Gupta, “A comprehensive study of ferromagnetic resonance and structural properties of iron-rich nickel ferrite ($\text{Ni}_x\text{Fe}_{3-x}\text{O}_4$, $x < 1$) films grown by chemical vapor deposition,” *Journal of Magnetism and Magnetic Materials*, vol. 417, pp. 137 – 142, 2016.
- [13] C. Kittel, “On the theory of ferromagnetic resonance absorption,” *Phys. Rev.*, vol. 73, pp. 155–161, Jan 1948.
- [14] J. Beik Mohammadi, J. M. Jones, S. Paul, B. Khodadadi, C. K. A. Mewes, T. Mewes, and C. Kaiser, “Broadband ferromagnetic resonance characterization of anisotropies and relaxation in exchange-biased IrMn/CoFe bilayers,” *Phys. Rev. B*, vol. 95, p. 064414, Feb 2017.
- [15] H. Xi, K. R. Mountfield, and R. M. White, “Ferromagnetic resonance studies of exchange biasing in $\text{Ni}_{81}\text{Fe}_{19}/\text{Pt}_{10}\text{Mn}_{90}$ bilayers,” *Journal of Applied Physics*, vol. 87, no. 9, pp. 4367–4374, 2000.
- [16] A. Layadi, W. Cain, J. . Lee, and J. Artman, “Investigation of anisotropy by ferromagnetic resonance (fmr) in exchange-coupled bilayer films,” *IEEE Transactions on Magnetics*, vol. 23, pp. 2993–2995, Sep. 1987.
- [17] C. K. Mewes and T. Mewes, “Relaxation in magnetic materials for spintronics,” *Handbook of Nanomagnetism*, pp. 71–96, 2015.
- [18] H. Suhl, “Ferromagnetic resonance in nickel ferrite between one and two kilomegacycles,” *Phys. Rev.*, vol. 97, pp. 555–557, Jan 1955.
- [19] B. Heinrich, J. F. Cochran, and R. Hasegawa, “Fmr linebroadening in metals due to two-magnon scattering,” *Journal of Applied Physics*, vol. 57, no. 8, pp. 3690–3692, 1985.
- [20] Z. Celinski and B. Heinrich, “Ferromagnetic resonance linewidth of fe ultrathin films grown on a bcc cu substrate,” *Journal of applied physics*, vol. 70, no. 10, pp. 5935–5937, 1991.
- [21] T. D. Rossing, “Resonance linewidth and anisotropy variation in thin films,” *Journal of Applied Physics*, vol. 34, no. 4, pp. 995–995, 1963.
- [22] R. Arias and D. Mills, “Extrinsic contributions to the ferromagnetic resonance response of ultrathin films,” *Physical review B*, vol. 60, no. 10, p. 7395, 1999.

- [23] A. M. Leary, P. R. Ohodnicki, M. E. McHenry, V. Keylin, J. Huth, and S. J. Kernion, “US20140338793A1 tunable anisotropy of Co-based nanocomposites for magnetic field sensing and inductor applications,” Jan 2019.
- [24] J. L. B.C. Dodrill and J. Krausen, “Magnetic anisotropy: Measurements with a vector vibrating sample magnetometer,” *Application Note, Lakeshore Cryogenics*, 2004.
- [25] J. Mohammadi, K. Cole, T. Mewes, and C. Mewes, “Inhomogeneous perpendicular magnetic anisotropy as a source of higher-order quasistatic and dynamic anisotropies,” *Physical Review B*, vol. 97, no. 1, p. 014434, 2018.
- [26] W. Sucksmith and J. E. Thompson, “The magnetic anisotropy of cobalt,” *Proceedings of the Royal Society of London. Series A. Mathematical and Physical Sciences*, vol. 225, no. 1162, pp. 362–375, 1954.
- [27] E. C. Stoner and E. P. Wohlfarth, “A mechanism of magnetic hysteresis in heterogeneous alloys,” *Philosophical Transactions of the Royal Society of London. Series A, Mathematical and Physical Sciences*, vol. 240, no. 826, pp. 599–642, 1948.
- [28] G. Herzer, “Modern soft magnets: Amorphous and nanocrystalline materials,” *Acta Materialia*, vol. 61, no. 3, pp. 718 – 734, 2013. The Diamond Jubilee Issue.
- [29] F. Luborsky and J. Becker, “Strain-induced anisotropy in amorphous alloys and the effect of toroid diameter on magnetic properties,” *IEEE Transactions on Magnetics*, vol. 15, no. 6, pp. 1939–1945, 1979.
- [30] W. Grimmond, A. J. Moses, and P. C. Ling, “Geometrical factors affecting magnetic properties of wound toroidal cores,” *IEEE Transactions on Magnetics*, vol. 25, no. 3, pp. 2686–2693, 1989.